Discovery of a star sensitive to the spin of Sgr A*

Stefan Gillessen

ste@mpe.mpg.de

MPE https://orcid.org/0000-0002-5708-0481

Physical Sciences - Article

Keywords: Galactic Center, massive black holes, general relativity, Kerr metric, stellar orbits

Posted Date: February 4th, 2026

DOI: https://doi.org/10.21203/rs.3.rs-8619199/v1

Additional Declarations: There is **NO** Competing Interest.

Discovery of a star sensitive to the spin of Sgr A*

K. Abd El Dayem[2], R. Abuter[7], N. Aimar[10,13], P. Amaro-Seoane[21,1], A. Berdeu[7,2], J.-P. Berger[4], G. Bourdarot[1], W. Brandner[5], A. Burkert[26,1], D. Calderon[24], C. Correia[10,13], J. Cuadra[22,23], R. Davies[1], D. Defrère[9], L. Delit[2], A. Drescher[4,1], F. Eisenhauer[1,12], L. Esteras Otal[7], M. Fabricius[1], H. Feuchtgruber[1], N.M. Förster Schreiber[1], A. Foschi[2], P. Garcia[10,13], R. Garcia Lopez[15], A. Generozov[18], R. Genzel[1,11], S. Gillessen[1], F. Gonté[7], X. Haubois[25], S.F. Hönig[8], M. Houllé[4], S. Joharle[1], A. Kaufer[25], J. Kammerer[7], P. Kervella[2], J. Kolb[7], L. Kreidberg[5], R. Laugier[9], S. Lacour[2], O. Lai[3], J.-B. Le Bouquin[4], J. Leftley[8], B. Lopez[3], D. Lutz[1], F. Mang[1,12,*], A. Mérand[7], F. Millour[3], M. Montargès[2], N. Morujão[10,13], H. Nowacki[3], M. Nowak[2], S. Oberti[7], J. Osorno[2,*], T. Ott[1], T. Paumard[2], C. Paladini[25], H.B. Perets[19], K. Perraut[4], G. Perrin[2], R. Petrov[3], P.O. Petrucci[4], T. Piran[20], N. Pourré[4], S. Rabien[1], D.C. Ribeiro[1], S. Robbe-Dubois[3], M. Sadun Bordoni[1], J. Sánchez Bermúdez[16], D. Santos[1], R. Sari[20], J. Sauter[5], S. Scheithauer[5], J. Scigliuto[3], J. Shangguan[1], T.T. Shimizu[1], F. Soulez[17], J. Stadler[24], C. Straubmeier[6], E. Sturm[1], M. Subroweit[6], C. Sykes[8], L.J. Tacconi[1], P. Thévenet[2], I. Urso[2], F. Vincent[2], J. Woillez[7], G. Zins[25]

(GRAVITY$^+$ Collaboration)

[1] *Max Planck Institute for Extraterrestrial Physics, Giessenbachstraße 1, 85748 Garching, Germany*

[2] *LIRA, Observatoire de Paris, Université PSL, CNRS, Sorbonne Université, Université de Paris, 5 place Jules Janssen, 92195 Meudon, France*

*Corresponding authors: F. Mang (fmang@mpe.mpg.de), J. Osorno (juan.osorno@obspm.fr), S. Gillessen (ste@mpe.mpg.de)

[3] *Université Côte d'Azur, Observatoire de la Côte d'Azur, CNRS, Laboratoire Lagrange, France*

[4] *Univ. Grenoble Alpes, CNRS, IPAG, 38000 Grenoble, France*

[5] *Max Planck Institute for Astronomy, Königstuhl 17, 69117 Heidelberg, Germany*

[6] *1st Institute of Physics, University of Cologne, Zülpicher Straße 77, 50937 Cologne, Germany*

[7] *European Southern Observatory, Karl-Schwarzschild-Straße 2, 85748 Garching, Germany*

[8] *School of Physics & Astronomy, University of Southampton, Southampton, SO17 1BJ, United Kingdom*

[9] *Institute of Astronomy, KU Leuven, Celestijnenlaan 200D, 3001, Leuven, Belgium*

[10] *Faculdade de Engenharia, Universidade do Porto, rua Dr. Roberto Frias, 4200-465 Porto, Portugal*

[11] *Departments of Physics & Astronomy, Le Conte Hall, University of California, Berkeley, CA 94720, USA*

[12] *Department of Physics, Technical University of Munich, 85748 Garching, Germany*

[13] *CENTRA - Centro de Astrofísica e Gravitação, IST, Universidade de Lisboa, 1049-001 Lisboa, Portugal*

[14] *Max Planck Institute for Radio Astronomy, auf dem Hügel 69, 53121 Bonn, Germany*

[15] *School of Physics, University College Dublin, Belfield, Dublin 4, Ireland*

[16] *Instituto de Astronomía, National Autonomous University of Mexico, Mexico City, Mexico*

[17] *Univ. Lyon, Univ. Lyon 1, ENS de Lyon, CNRS, Centre de Recherche Astrophysique de Lyon UMR5574, F-69230, Saint Genis-Laval, France*

[18] *Astronomy Dept. and Oden Institute, University of Texas at Austin, Austin, TX 78712, USA*

[19] *Physics department, Technion - Israel Institute of Technology, Technion city, Haifa 3200002, Israel*

[20] *Racah Institute of Physics, The Hebrew University, Jerusalem 91904, Israel*

[21] *Universitat Politècnica de València, C/Vera s/n, València, 46022, Spain*

[22] *Universidad Adolfo Ibañez, Av. Padre Hurtado 750, Viña del Mar, Chile*

[23] *Millennium Nucleus on Transversal Research and Technology to Explore Supermassive Black Holes (TITANS), Chile*

[24] *Max Planck Institute for Astrophysics, Karl-Schwarzschild-Straße 1, 85748 Garching, Germany*

[25] *European Southern Observatory, Casilla 19001, Santiago 19, Chile*

[26] *University Observatory, Faculty of Physics, Ludwig-Maximilians-Universität, Scheinerstraße 1, 81679 Munich, Germany*

Abstract

Residing in the center of the Milky Way, Sgr A* is the closest massive black hole. Its vicinity has allowed measuring individual stellar orbits around it with periods as short as 12 years. The stars act as test particles and probe the gravitational potential around the $\mathbf{4.3 \times 10^6} M_\odot$ black hole. These observations have determined the central mass to sub-percent precision, and the mildly relativistic motions of stars have given access to seeing the dominant relativistic corrections, the gravitational redshift, the transverse Doppler effect and the prograde precession imposed by the Schwarzschild metric nature of the potential. These effects are of order $\boldsymbol{(v/c)^2}$ (for velocity $\boldsymbol{v}$ and speed of light $\boldsymbol{c}$). The Kerr metric occurring for a rotating black hole leads to corrections of order $\boldsymbol{(v/c)^3}$. Here, we report the discovery of a faint main sequence star ($\boldsymbol{m_K = 19.3}$), S301, the orbit of which has a period of 8.7 years and small enough a pericenter distance, such that the star's peak velocity reaches **25000** km/s or 8% of $\boldsymbol{c}$. Within the measurement capabilities of current near-infrared interferometry and future spectroscopy on an extremely large telescope, S301's motion is directly sensitive to the spin of Sgr A*. The high eccentricity of S301 suggests that it is the captured component of a binary that was torn apart via the Hills mechanism, sending the other component away as a hyper-velocity star.

Keywords: Galactic Center, massive black holes, general relativity, Kerr metric, stellar orbits

1 Introduction

A black hole in general relativity has just two additional degrees of freedom beyond its mass: spin and charge. Astrophysically relevant is the spin. As all objects in the Universe rotate, one would expect the same for black holes, in particular, since the angular momentum of material creating a black hole needs to be conserved. The existence of jets in active galactic nuclei requires that the black holes located in the central engines rotate [1]. As the effects of the spin on space-time fall off with distance r to the black hole like r^{-3}, it is actually hard to measure a spin. Spin estimates have been obtained from X-ray reflection spectra, in which the iron K-α line shape is a probe of the spin, albeit the spin's impact is small [2]. For accreting stellar-mass black holes, spins can be estimated from accretion theory [3], and thus are not assumption-free. The cleanest signatures are probably those of gravitational wave mergers, in which the spins of the initial objects are among the fit parameters to the pre-mergers wave forms [4] and the spin of the resulting black hole can be inferred from its ringdown signature [5]. The space experiment Gravity Probe B detected the spin-induced precession due to Earth twisting space-time with 5σ significance [6], testing the far-field and slow-motion approximation around a massive body, which equals the approximation of the Kerr metric in the same limit [7]. Overall, there are only few current observational constraints on the spin parameter of the Kerr metric.

Sgr A*, the closest massive black hole (MBH) in the Galactic Center at a mere distance of 8.3 kpc offers a direct, dynamical way to measure its spin. The observation

of stellar orbits has allowed measuring its mass to the sub-percent level, making Sgr A* one of the best cases for the existence of black holes in general [8]. A few dozen stars revolve on (nearly) Keplerian orbits, with an almost thermal, relaxed eccentricity distribution and randomly oriented orbital planes. Most valuable are the stars that come closest to Sgr A*, as they probe deepest into the gravitational potential. In particular the star S2 on a 16-year orbit [9] has been in focus, due to its comparably easily accessible orbit. The observed motion of S2 is notably affected by relativistic effects: During its 2018 pericenter passage, the gravitational redshift of Sgr A* led to an additional change of measured atomic line positions of around 200 km/s [10]. By 2020, the astrometric data of the star showed that the orbit had changed at pericenter the orientation of the ellipse in the orbital plane by around 12', fully consistent with the general relativistic expectation for a motion in the Schwarzschild metric [11, 12]. In the sense of a Post-Newtonian expansion, both relativistic effects are of order $\beta^2 = (v/c)^2$. Key for these discoveries was the advent of near-infrared interferometry using 8m-class telescopes, namely the GRAVITY instrument in operation at the European Southern Observatory's (ESO) Very Large Telescope (VLT) [13]. At the β^3 order, the leading-order term from the Kerr metric contributes. At that order the motion will thus be sensitive to the spin of Sgr A*, often called 'Lense-Thirring' precession [14].

For S2, current instrumentation would require prohibitively long time series to detect the spin. The parameter determining how sensitive a star is to relativistic effects is the pericenter distance r_p [15], which for S2 is $1400\,R_S$ (Schwarzschild radii). Stars with smaller r_p would allow a quicker detection. Since $r_p = a(1-e)$, this requires smaller semi-major axes a and/or larger eccentricities e. For the mass of Sgr A* of $4.3 \times 10^6 M_\odot$ and its distance of 8.3 kpc, $1R_S = 10\,\mu$as. This is comparable to the astrometric precision of $\simeq 30\,\mu$as for S2 of GRAVITY. Together with the spatial resolution as good as ≈ 1.7 mas and a field of view of around $r = 70$ mas, it is clear that GRAVITY can trace the pericenter passages of stars that come much closer to Sgr A* than S2. The newly discovered star S301 presented here is a first and already prime example for this, as it constitutes exactly the type of relativistic test particle required for a spin measurement of Sgr A* on a 10-year time scale. Further, we discuss the astrophysical implications of its extremely eccentric orbit, pointing to an origin via the Hills mechanism [16].

2 Observations & data analysis

Since 2017, we have regularly observed the central arcsecond around Sgr A* with GRAVITY with the purpose of tracking the stellar motions. Observations take place during roughly week-long campaigns, placed monthly around full-moon, during the months in which Sgr A* is observable between March and September. A total of around 80-100 hours per year of observing time is used for that. A major part of the integration time is spent on a central pointing containing Sgr A* itself, as this serves as astrometric reference for all stellar positions. The data consist per 360 s exposure of a set of complex visibilities for six baselines, recorded on 14 spectral channels (of which 12 are usable) for each of two linear polarizations (Fig. B1).

Typically, we group the data per night and analyze the data sets in two ways: First, we fit a model to them. It contains the known sources and returns positions and fluxes of these. By design, this does not reveal new sources. Hence, in a second step, we employ image reconstruction techniques to Fourier-invert the data into an image. Beyond classical algorithms developed in the context of radio interferometry like CLEAN, we use our own code 'GRAVITY-RESOLVE', G^R ([17, 18], Appendix B.1). The images obtained allow identifying previously unknown sources (Fig. 1).

In spring 2023, we discovered a faint star just 15 mas north-west of Sgr A*, which in the following months quickly moved outward, and which we labeled S301. We obtained a total of four positions in 2023, indicating a quick and slightly curved motion, that would bring the star by 2024 outside of the central field of view. Consequently, we decided to follow the star with dedicated pointings in 2024 and 2025, yielding eight and five additional astrometric measurements of S301 respectively.

With a preliminary orbit in hand, we were also able to post-dict where the star should have been in previous observing epochs, and whether it would be by chance in one of our pointings from previous years. It turns out that we found a strong inference of S301 in 2021 and a weak inference in 2017. These positions are less certain, as only a few exposures at the respective pointings were taken. Overall, we have thus 19 astrometric positions of S301 that consistently outline an elliptical figure on the sky.

We have tried to identify the star in deep ERIS integral-field spectroscopic data, but have not been able to detect it as a continuum source or from spectral features, such as the hydrogen Brackett-γ line at 2.1661 μm, or the CO-band head features redwards of 2.2935 μm. We thus do not yet have any radial velocity information.

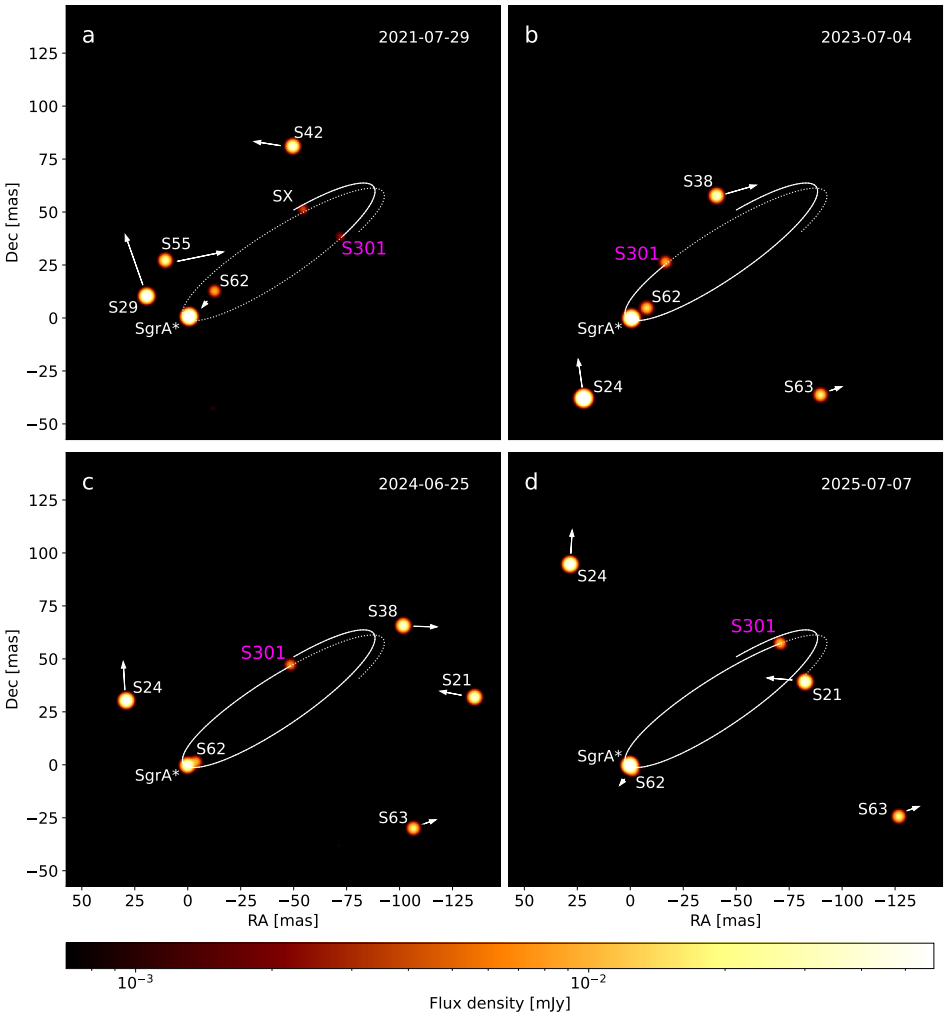

Fig. 1 Time series of GRAVITY Galactic Center images from 2021 to 2025, reconstructed with G^R (see appendix B.1 for details). The objects are labeled by their names, and for S301 the orbital trace (Fig. 2) is shown on top. In panels **c** and **d** Sgr A* and S62 are confused. SX is a potential source not yet named or otherwise identified.

3 Results

From the GRAVITY images, we measure the positions of S301 and Sgr A* to obtain the position vector for the star relative to the central mass. For observations, in which the S301 pointing was not centered on Sgr A* (in 2024 and 2025, as well as in 2021 and 2017), the two objects are fitted relative to their respective field centers. The positional offset between the latter two is measured at the interferometric precision by

GRAVITY's metrology system. Our imaging code G^R also allows estimating the uncertainties in the positions, as multiple instances of the same images are inferred, from which standard statistical methods yield averages as well as uncertainty estimates.

The brightness of the objects inferred is measured by the fluxes of the sources in the images. In all images, brighter stars are present for which photometry as used in [19] is available. For S301, we derive a K-band magnitude of $m_K = 19.3 \pm 0.3$.

Using a standard-χ^2 minimization technique, we fit a preliminary Keplerian orbit to the astrometric data $\alpha(t)$ and $\delta(t)$. According to this fit, the star passed the pericenter of its orbit at the beginning of 2023, with a 3D separation significantly smaller than that of S2. Hence, we need to take into account the β^2 relativistic effects, using the same model as for S2 in Gravity Collaboration et al. [11], including thus the Rømer effect (retardation effects due to the finite speed of light) and Schwarzschild precession as predicted by general relativity. The potential is defined by the central mass fixed with $M_{\mathrm{MBH}} = 4.297 \times 10^6 M_\odot$ at a distance of $R_0 = 8277\,\mathrm{pc}$. We do not allow for any coordinate system offsets, as our data are interferometrically referenced directly to the near-infrared counterpart of Sgr A*.

Due to the lack of radial velocity information, two equally valid solutions exist, corresponding to the two possible orientations of the orbit. In principle, the Rømer delay could break this degeneracy [20], but the two orbit orientations yield indistinguishable best-fit χ^2 values. Except for this sign ambiguity, the orbit fit converges uniquely (as verified by sampling the posterior space with a Markov chain Monte Carlo) at $\chi^2 = 29.1$ for 34 degrees of freedom. The orbit does not agree with any previously claimed detections (see appendix F).

The best-fit orbit is remarkable (table C2) with a semi-major axis of $a = 83\,\mathrm{mas}$ (33% smaller than S2's orbit) and an orbital period of 8.7 years, see Fig. 2. The star sets thus a new record for the shortest known orbital period around Sgr A*, with S55 / S0-102 on a 12-year orbit [21] being the previous record-holder. Even more extreme is the eccentricity of $e = 0.9825/0.9816$ (for the two possible orbit orientations), leading to a pericenter distance $r_p = a(1-e)$ of only $140/149\,R_S$, i.e. around ten times smaller than S2's. This leads to correspondingly stronger relativistic effects. The relativistic pericenter advance per orbit amounts to $1.9°/1.8°$, such that after only 1630 / 1710 years the orientation of the orbit in its plane has revolved once. At pericenter, S301 moves with $\approx 25\,000\,\mathrm{km\ s^{-1}}$ / $24\,400\,\mathrm{km\ s^{-1}}$ or 8.3% / 8.1% of c.

4 Discussion

4.1 Stellar type

Given the magnitude of $m_K = 19.3$ and the associated uncertainty of 0.3 mag, assuming an extinction of 2.42 [22] and a Galactic Center distance of 8.3 kpc [20], S301 has an absolute K magnitude of around 2.28. It is too faint to be a giant, but it instead is compatible with being a main sequence star. Its spectral type then is a late A-type or an early F-type star (see also Fig. 2 in [23]), which means its color index $V - K = 0.6$ [24]. With a V magnitude of 2.88 it has $L = 5.5\,L_\odot$ and a spectral type of F1.5, corresponding to a mass of just below $1.5\,M_\odot$. Alternatively, the stellar mass can be estimated from stellar evolutionary tracks to be between $\sim 1.1 M_\odot$ and

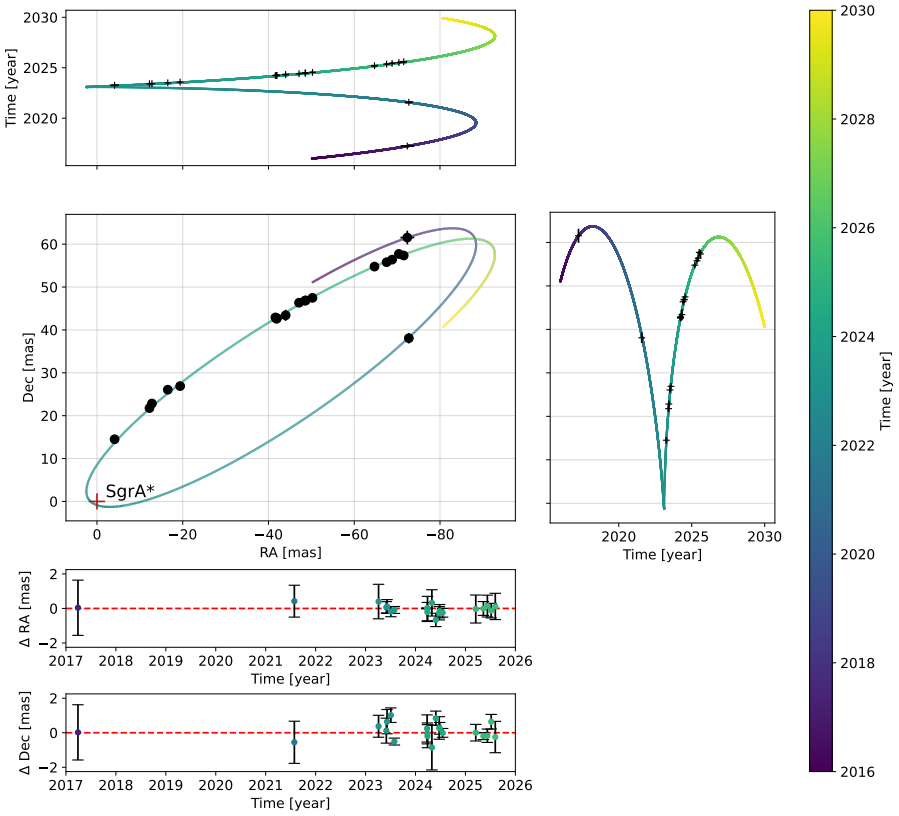

Fig. 2 Orbit of S301 over the course of 14 years. The central panel shows the best-fit relativistic orbit to individual positions of S301 in a Schwarzschild metric around Sgr A* (see appendix C for details). Adjacent panels to the top and right show its proper motion over time separately in RA and Dec, respectively. Corresponding residuals in the bottom two panels reveal a well-matched orbit to the astrometry. Due to the high eccentricity and short semi-major axis of S301, its orbit visibly does not close as a result of the Schwarzschild precession.

$\sim 1.5 M_\odot$, depending on the age of the star, with younger ages corresponding to larger masses (appendix D). S301's radius should be between $\sim 1.4\,R_\odot$ and $\sim 1.6\,R_\odot$. The main-sequence life time of early F-type stars is around 2×10^9 yr.

Spectrally, we therefore expect S301 to show exclusively the Brackett-γ absorption line, but no further features [25]. Our current ERIS spectroscopy is not deep enough to test this prediction. Future MICADO [26] spectroscopy at the ELT will have no

problem in seeing the spectral feature(s) of S301 and thus will be able to determine the radial velocity.

A second argument can be made from the fact that S301 apparently did not get tidally disrupted at pericenter. A giant star with $r_* = 0.5\,\mathrm{AU}$ and $m_* = 3\,M_\odot$ begins to lose a fraction of its envelope at its tidal radius $r_t = r_*(m_*/M_{\rm MBH})^{1/3} \approx 500\,R_S > r_p$. The loss of some mass will surely affect the orbit at pericenter and this is not observed. On the other hand, for a main sequence star $r_t \approx 10\,R_S$. Hence, given its orbit and demanding tidal stability, S301 cannot be a giant star, but it is safe from tidal disruption if it is a dwarf. In Appendix E we show that also tidal heating is not a major effect for S301. Interestingly [27] suggest that these tidal effects will prevent observations of Kerr effects around Sgr A*. However, they consider stars 10 $M_\odot$ or heavier. S301 is sufficiently small so that these tidal effects are negligible.

4.2 Spin sensitivity

The most exciting aspect of S301's orbit is its extremely small pericenter distance, such that it is sensitive to the spin of Sgr A* to a degree accessible within a reasonable time scale of around a decade, using existing and/or planned instrumentation. Fig. 3 (left) predicts for a "randomly" oriented ($\lambda = \beta = 0$), but maximally rotating black hole spin ($\chi = 1$; where $\chi \equiv cJ/(GM_{\rm MBH}^2)$ is the dimensionless spin parameter) the precession effects on the orientation of the orbit in its plane. The dominant effect is the Schwarzschild precession, advancing the pericenter by 1.9° per revolution. The orbit-averaged Lense-Thirring effects for the in-plane and out-of-plane major axis precession are respectively [28, 29]

$$\begin{aligned} \Delta\varpi_{\rm LT} &= -8\pi\chi\cos\beta\left(\frac{GM_{\rm MBH}}{a(1-e^2)}\right)^{3/2}\,, \\ \Delta\Theta_{\rm LT} &= -4\pi\chi\sin\beta\sin\lambda\left(\frac{GM_{\rm MBH}}{a(1-e^2)}\right)^{3/2}\,, \end{aligned} \tag{1}$$

where β is the inclination between spin axis and orbital angular momentum, and λ is the position angle of the projection of the spin axis onto the orbital plane. For S301, the in-plane contribution evaluates to $0.11°\chi\cos\beta$ per revolution, comparable to the angle S2's orbit advances due to the Schwarzschild metric, and which we have measured using GRAVITY data in [11]. The Schwarzschild precession will lead to a full turn of the ellipse within 1630 years only, and the time scale for the spin precession [30] is 58000 years.

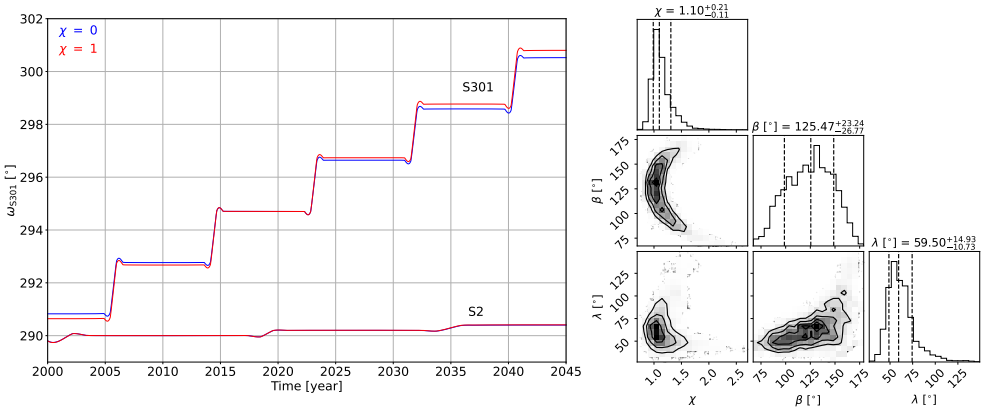

Fig. 3 Left: Change of the orientation of the orbital ellipse (measured by the osculating orbital parameter longitude of pericenter ω) as a function of time for S301 in comparison with S2. The discrete steps occur when the respective star passes the pericenter of its orbit. The blue lines are for a non-rotating Schwarzschild metric ($\chi = 0$), the red ones correspond to a "randomly" oriented ($\lambda = \beta = 0$, pointing towards the Sun), maximally spinning black hole. The extra-precession due to the spin of Sgr A* of the S301 orbit is of similar magnitude as the changes induced by the 1PN-terms of the Schwarzschild metric of S2, which have been detected already [11, 12]. Right: Example of constraints on the spin parameters (χ, λ, β) for a mock data set with future simulated data up to 2035 (for details see text). The mock data in this case constrain the spin magnitude χ with an uncertainty < 0.2, and also the orientation to around $\pm 30°$.

In order to assess how S301 can be used to probe the spin of Sgr A*, we perform a mock data analysis combining current and simulated future observations. We construct synthetic astrometric and radial-velocity datasets extending the existing measurements with simulated observations between 2026 and 2035, using the values of the orbital parameters given in table C2, with mass and distance of Sgr A* from [12]. We optimistically adopt $\chi = 1$ and an orientation approximately aligned with the stellar orbital angular momentum. In this case, the Lense-Thirring effect produces mainly in-plane precession and little precession of the orbital plane. The resulting mock orbit is fitted to test whether the spin parameters can be recovered. We assume a realistic astrometric precision of 100 μas and 1 km/s accuracy on the radial velocity as reachable with future ELT/MICADO observations. A sampling of 10 data points per year until 2035, with 10 additional data points around pericenter, would yield a spin constraint with an uncertainty on χ of around 0.1 (Fig. 3, right), equivalent to a $> 5\sigma$ detection of $\chi = 1$ compared to the non-spinning ($\chi = 0$) case. In Fig. 4 we show the dependence of the significance of the spin detection in our simulations as a function of orientation of the black hole spin. The maxima of significance correspond to (anti-)alignment of the spin and orbital angular momentum, while the minima correspond to alignment of the spin along the semi-major axis of the orbit. A more detailed discussion is provided in [31].

S301 therefore provides the first and currently only practical way to measure the spin of Sgr A* with stellar dynamics. Continued GRAVITY+ astrometry and future ELT spectroscopy can turn S301 into a spin probe. While S2 and the other known

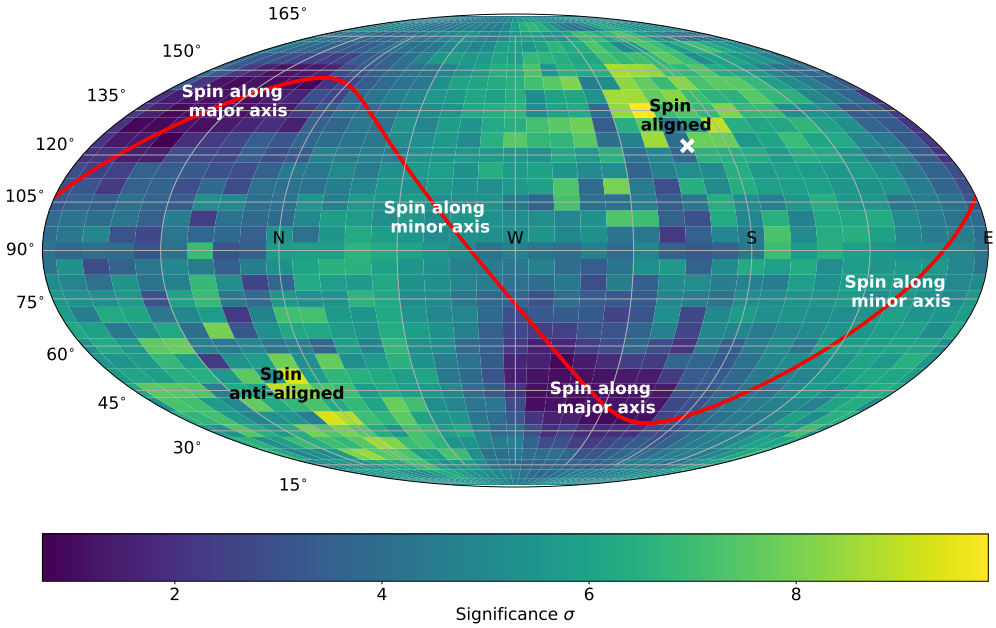

Fig. 4 Significance of the detection of the spin as a function of orientation of the spin vector for our simulated data with $\chi = 1$. Over a wide range of possible orientations, we expect to be able to detect the spin. The cross marks the orientation of the orbital angular momentum vector of S301. The red line corresponds to maximum misalignment between black hole spin and orbit. The best chances of detection are for co- or anti-alignment.

S-stars owed to their larger pericenter distances are effectively insensitive to frame dragging on observationally accessible time scales, they will provide constraints on $M_{\rm MBH}$ and R_0, which can be used as external priors, reducing degeneracies and assisting the measurement of the spin magnitude and, eventually, of its orientation. Newtonian perturbations due to dark masses orbiting Sgr A* are expected to be subdominant (appendix G). In the longer term, S301 opens a path towards constraining the quadrupole moment of Sgr A* and testing the Kerr no-hair relation [32] once sufficiently long time series of sufficiently accurate astrometry and spectroscopy become available.

4.3 Origin of S301

Another interesting aspect of the orbit is its history. As we discuss in more detail in Appendix H, the star and its orbit can be affected by stellar collisions and relaxation. Since star formation so close to the MBH is unlikely given the strong tidal effect by the MBH, S301 has likely formed elsewhere and migrated to its current location. Given its estimated mass, the life time of S301 is comparable to the two-body relaxation time, and it is therefore unlikely to have formed in the nuclear cluster and slowly migrated inwards through two-body relaxation.

Table 1 Time scales (in years) for S301 and S2. $T_{\rm orb}$ is the orbital period. $T_{\rm SP}$ is the time scale for the Schwarzschild precession, $T_{\rm LT}$ for Lense-Thirring precession [33]. $T_{\rm Vec-RLX}$ refers to the angular momentum relaxation time scale, estimated both with and without resonant relaxation ('RR' and 'No RR' respectively). $T_{\rm Sca-RLX}$ refers to the energy relaxation time scale. $T_{\rm coll,bh}$ and $T_{\rm coll,\star}$ are the collision time scales with background black holes and stars respectively. The collision and relaxation times are estimated for relaxed stellar density profiles, as described in appendix H. The gravitational wave inspiral time scale $T_{\rm GW}$ is given by [34], and the energy dissipation time scale $T_{\rm heat}$ by [35] (see appendix E). For these estimates we assume $1.5M_\odot$ and $1.4R_\odot$ for the stellar mass and radius of S301, and $15M_\odot$ and $4.7R_\odot$ for S2.

Time scale [yr]	S301	S2
$T_{\rm orb}$	8.7	16.1
$T_{\rm SP}$	1.6×10^3	2.8×10^4
$T_{\rm LT}$	5.8×10^4	3.1×10^6
$T_{\rm Vec-RLX}$ (No RR)	2.5×10^7	2.3×10^8
$T_{\rm Vec-RLX}$ (RR)	2.0×10^7	3.6×10^7
$T_{\rm Sca-RLX}$	8.6×10^8	1.1×10^9
$T_{\rm coll,bh}$	1.8×10^9	4.0×10^8
$T_{\rm coll,\star}$	1.7×10^8	4.6×10^7
$T_{\rm GW}$	2.9×10^{10}	7.1×10^{12}
$T_{\rm heat}$	3×10^{16}	2×10^{29}

Instead, the extreme value $e \simeq 0.98$ is naturally produced in a short-time dynamical migration scenario through a Hills disruption of a compact main-sequence binary by the MBH [16, 36–40].

For the Hills mechanism the star is captured at a semi-major axis of

$$a_{\rm cap} = f_1 \left(\frac{M_{\rm MBH}}{m_{\rm bin}} \right)^{2/3} a_{\rm bin}, \tag{2}$$

where $f_1 \approx 0.5$ for circular, equal mass binaries [e.g. 41]. The captured star will inherit the pericenter of the binarys orbit around the MBH, and so the binary separation must be no more than a factor few times $(M_{\rm MBH}/m_{\rm bin})^{1/3}\, a_{\rm bin}$ (the characteristic binary tidal disruption radius). Thus, the eccentricity of the captured star will be

$$e_{\rm cap} = 1 - f_2 \left(\frac{m_{\rm bin}}{M_{\rm MBH}} \right)^{1/3}, \tag{3}$$

where f_2 is at most a factor of order unity. The expected distribution of f_2 and hence of $e_{\rm cap}$ will depend on the distribution of binary properties (e.g. the mass ratio, inclination, internal eccentricity) and the pericenter distribution of disrupting binaries. Recently, [42] simulated binary disruptions in the Galactic Center for an observationally motivated binary population, assuming a full loss cone and an isotropic inclination distribution. For captured stars with semi-major axes between 2×10^{-3} pc and 4×10^{-3} pc and masses between $1.3M_\odot$ and $1.7M_\odot$ the eccentricities ranged

between 0.97-0.996 (5th-95th percentile) with a median eccentricity of 0.985. Thus, binary disruption would naturally explain the observed eccentricity of the star.

As shown in Table 1 the angular momentum relaxation and collision time scales are expected to be less than the main sequence lifetime of the star. If the star has been in the Galactic Center for a few $\times 10^7$ yr or longer we would expect its eccentricity to have thermalized, losing memory of its initial condition. In this case, the high, observed eccentricity simply occurs by chance (quantitatively, there is a $\sim 3\%$ chance to have an eccentricity as high as that of S301 for a thermal distribution). Alternatively S301 may have been injected into the Galactic Center in the recent past, so that it has not had time to relax. Finally, we highlight that our estimates of the relaxation times are sensitive to the assumed background density profiles. The relaxation times may be significantly longer if there is a dearth of stellar mass black holes at the radial regime of S301.

The measured semi-major axis constrains the pre-disruption binary. For nearly equal masses the Hills mapping gives $a_{\rm cap} \sim \frac{1}{2}(M_{\rm MBH}/2m_*)^{2/3} a_{\rm bin}$ [e.g. 41]. Identifying $a_{\rm cap} \simeq a$ and adopting $m_* \simeq 1.3$–$1.7\,M_\odot$ yields a pre-disruption separation $a_{\rm bin} \sim 0.05$–0.2 AU, corresponding to orbital periods $P_{\rm bin} \sim 5$–20 days. We find a similar range of progenitor semi-major axes in the simulations of [42], with an observationally motivated mass ratio distribution.

Such compact binaries are common among F-type stars [43] and are expected to be tidally circularised and nearly synchronised. If S301 was initially synchronised, its spin period at capture would have been comparable to $P_{\rm bin}$, implying an equatorial rotation velocity $v_{\rm rot} \sim 20$–$70\ {\rm km\,s^{-1}}$ for $R_* \simeq 1.3$–$1.7\,R_\odot$. High-resolution spectroscopy with ERIS or ELT/MICADO might therefore provide a direct, testable prediction of the Hills-binary origin via a measurement of $v \sin i$.

Taken together, the properties of S301 suggest a simple and self-consistent picture: a compact main-sequence binary was tidally separated by Sgr A*, leaving behind S301 on the most relativistic stellar orbit known and ejecting its companion as a hyper-velocity star. Such events simultaneously populate the innermost S-star cluster and the halo hyper-velocity star population. For Hills disruption rates of order $\dot{N}_{\rm Hills} \sim 10^{-5}$–$10^{-4}\,{\rm yr^{-1}}$, simple steady-state arguments suggest that one expects of order a few S301-like stars on similarly relativistic orbits at any given time. The Hills disruption rate is supported by both the observed number of hyper-velocity stars in our galaxy [44] and theoretical estimates as well as the observed tidal disruption rate in other galaxies. With roughly 10% of them having the right separation range to produce S301 like orbits (see equation 2 above), we take the formation rate of stars on S301 like orbits to be $\dot{N}_{S301} \sim 10^{-6}$. Given the collisional lifetime of more than 10^8 years (see table 1), we expect in steady state about a hundred stars with such an orbit. Most of them are likely solar mass stars, and hence still too faint to be detected. Further analysis of the observed coverage and current sensitivities of GRAVITY+ is needed to assess if this estimate is consistent with only one S301-like object detected so far; and continued GRAVITY+ monitoring and future ELT observations may therefore reveal a population of faint, low-mass S-stars deep in the potential well, enabling ensemble constraints on the spin of Sgr A* and on the distribution of stellar and remnant perturbers in the innermost $\sim 10^{-2}$ pc.

4.4 Summary and implications

S301 is, at present, the most extreme stellar test particle known around Sgr A*. Its very short period, small semi-major axis and pericenter at $\simeq 140\,R_{\rm S}$ place it well inside the regime where relativistic precession dominates over Newtonian perturbations from the surrounding cluster. Together with the clean astrometric reference provided by GRAVITY, this makes S301 uniquely sensitive to the Lense-Thirring terms of the Kerr metric and therefore to the spin of the Galactic Center black hole. Our mock-data analysis shows that continued GRAVITY monitoring at current precision is sufficient to detect the in-plane Lense-Thirring precession of S301's orbit on a time scale of around a decade, providing the first realistic opportunity to dynamically measure the spin of Sgr A* or of any massive black hole.

The photometry of S301, combined with its survival against tidal disruption at pericenter, establishes it as a compact, $\sim 1.5\,M_{\odot}$ main-sequence F-type star. The stars large present-day eccentricity is consistent with injection in the Galactic Center via the Hills mechanism.

The timescale hierarchy at S301s radius, with $T_{\rm orb} \ll T_{\rm SP} \ll T_{\rm LT} \ll T_{\rm Vec-RLX} \ll T_{\rm coll}, T_{\rm Sca-RLX} \ll T_{\rm GW}$ helps constrain its origin and evolution. The long two-body relaxation and gravitational wave inspiral times imply that the stars semi-major axis has not evolved significantly over its lifetime, and thus its present-day orbit constrains the progenitor binary, indicating it was compact with a period of 5–20 days.

Eccentricity evolution and stellar collisions can occur over the stars main sequence lifetime. However, its high eccentricity hints that its angular momentum has not had a chance to relax. This could occur if the star has been injected into the Galactic Center in the recent past or if background density at the relevant radii is far from a relaxed steady state. In this case S301 would be an almost pristine fossil of its capture event, evolving in a gravitational potential that is very nearly that of an isolated Kerr black hole.

Acknowledgements. We are very grateful to our funding agencies (MPG, ERC, CNRS [PNCG, PNGRAM], DFG, BMBF/BMFTR, Paris Observatory [CS, PhyFOG], Observatoire des Sciences de l'Univers de Grenoble, and the Fundação para a Ciência e a Tecnologia), to ESO and the Paranal staff, and to the many scientific and technical staff members in our institutions, who helped to make NACO, SINFONI, ERIS and GRAVITY/GRAVITY+ a reality. This project has received funding from the European Union's Horizon 2020 research and innovation programme under the Marie Sklodowska-Curie grant agreement No 101007855. This work was supported by Paris Île-de-France Region and by the French National Research Agency (ANR) under grant ANR-23-EDIR-0003 (GRAFITY). We acknowledge the financial support provided by FCT/Portugal through grants 2022.01324.PTDC, PTDC/FIS-AST/7002/2020, UIDB/00099/2020 and UIDB/04459/2020. TPiran acknowledges support from an advanced ERC grant MultiJets and from the Simons foundation SCEECS collaboration. The research of DCalderon has been funded by the Alexander von Humboldt Foundation. JStadler acknowledges funding from the Deutsche Forschungsgemeinschaft (DFG, German Research Foundation) under its Emmy-Noether Programm (STA 1955/1-1, Projektnummer 545534254). Based on observations collected at the European Southern Observatory under the ESO programme IDs 60.A-9102(A), 105.20B2.004, 111.24H1.00[123], 112.25CV.001, 113.268P.00[1234], 114.270V.001, 115.27WT.00[1234].

Appendix A Data

Our observations, from which we inferred S301, comprise 19 datasets spanning more than eight years. We first noted S301 in 2023, when pointing directly to Sgr A*. Given the star's position close to Sgr A* and its large proper motion, it was quickly clear that it might be on a tight orbit, and we followed up with dedicated observing campaigns over the course of the next years. We summarize the data used for this work in Table A1.

Table A1 Summary of GRAVITY data that yielded an inference of S301. The date in the first column follows ESO convention and gives the date of the evening of respective observing night. The epoch is the mean over the time stamps of the N_{exp} individual GRAVITY exposures. The total accumulated integration time per night is given by t_{int}, and $\mathbf{p}$ is the center of the individual pointings with respect to Sgr A*. All data were acquired in low-resolution mode and in two linear polarizations, except for the 2017 dataset, which was partially acquired with both polarizations combined.

Date	Epoch	N_{exp}	t_{int} [h]	$\mathbf{p}$ [mas]	program ID
2017-03	2017.2389	12 (one pol.)	1.0	$(-57.974, 35.939)$	60.A-9102(A)
2021-07-29	2021.5759	8	0.71	$(-45., 45.)$	105.20B2.004
2023-04-05	2023.2604	12	1.2	$(0.0, 0.0)$	111.24H1.001
2023-06-01	2023.4162	13	1.3	$(0.0, 0.0)$	111.24H1.002
2023-06-06	2023.4298	9	0.9	$(0.0, 0.0)$	111.24H1.002
2023-07-04	2023.5063	16	1.6	$(0.0, 0.0)$	111.24H1.003
2024-03-25	2024.2325	3	0.3	$(-51.13, 54.59)$	112.25CV.001
2024-03-27	2024.2380	2	0.2	$(-51.13, 54.59)$	112.25CV.001
2024-03-28	2024.2405	6	0.6	$(-51.13, 54.59)$	112.25CV.001
2024-04-29	2024.3281	4	0.4	$(-56.13, 59.59)$	113.268P.001
2024-05-28	2024.4073	12	1.2	$(-63.08, 63.25)$	113.268P.002
2024-06-22	2024.4756	10	1.0	$(-63.08, 63.25)$	113.268P.003
2024-06-25	2024.4837	9	0.9	$(-63.08, 63.25)$	113.268P.003
2024-07-17	2024.5438	9	0.9	$(-63.08, 63.25)$	113.268P.004
2025-03-16	2025.2070	10	1.0	$(-61., 51.2)$	114.270V.001
2025-05-11	2025.3602	10	1.0	$(-95.26, 51.2)$	115.27WT.001
2025-06-09	2025.4393	10	1.0	$(-95.26, 51.2)$	115.27WT.002
2025-07-07	2025.5159	9	0.9	$(-69.959, 56.581)$	115.27WT.003
2025-08-06	2025.5978	7	0.7	$(-72.005, 57.737)$	115.27WT.004

Based on the orbital coverage from 2023-2025, we were able to trace S301 back in time, and identified two previously acquired datasets in 2017 and 2021, in which the star should be present.

The 2017 data were acquired as part of the monitoring of the motion of the star S2, an object around five magnitudes brighter than S301. The dataset consists of individual exposures across five consecutive nights in March 2017, partially recorded in split-polarization mode. In the image reconstruction of this dataset, we treat both polarizations in polarized exposures as individual measurements and combine them with the unpolarized data.

The dataset in 2021 was acquired during an observation that involved multiple other pointings in the GC to create a mosaic of the central $\simeq 200 \times 200$ mas [17]. This particular pointing was affected by bad seeing conditions, however, and initially no

source was inferred in the corresponding reconstructed image [17]. Now, we apply stricter cuts and accept as a post-processing step only fringe-tracking ratios of 90 % for the individual detector integrations, effectively discarding data with low coherent flux. This procedure led to the inference of S301 in this particular epoch.

Appendix B Methods

B.1 Highest-resolution, deep images of the central 800 AU

The high-angular-resolution, high-fidelity images of the Galactic Center are reconstructed from GRAVITY data, an example of which is shown in Fig. B1 with the image reconstruction tool GRAVITY-RESOLVE (G^R) [17]. This code is designed to reconstruct stars in the Galactic Center that appear to GRAVITY as unresolved point sources and, in particular, to find faint, yet undiscovered stars. G^R is based on a hierarchical forward model that incorporates the instrument response of GRAVITY including both optical aberrations and the spectral transmission within the beam combiner, as well as a statistical model of the Galactic Center. The intrinsic multitude of degrees of freedom of an image is tamed with Bayesian inference, where the statistical model of the Galactic Center provides the prior information. With G^R, we exploit GRAVITY's supreme imaging resolution of $\simeq 1.7$ mas and its phase-referencing capabilities, which allow for high contrast images and routine mosaicking as pioneered in radio interferometry [18].
The individual positions of S301 over time, as depicted in Fig. 2, were inferred in a first step from imaging. We initialized the model in G^R by invoking all known, bright sources within the field of view. Positions and flux of the stars and Sgr A* are constrained by prior distributions that reflect current knowledge. We applied G^R a total of ten times to the same dataset with varying initial random seeds. Tentative faint sources that may appear in the image of individual reconstructions are only accepted when they are inferred in at least five out of ten reconstructions. Their corresponding positions in the image grid are then referenced to SgrA* and subsequently averaged. These positions provide the starting value for fitting routines, which infer the astrometry and photometry of S301 in a parameterized model, taking full advantage of GRAVITY's unmatched astrometric precision.

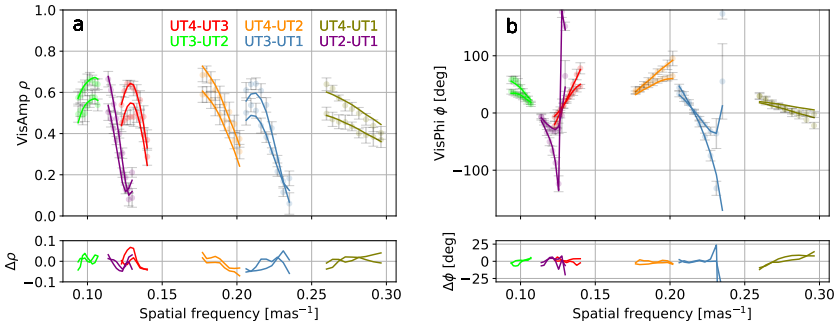

Fig. B1 GRAVITY Galactic Center data, showing the complex visibility samples of a single GRAVITY exposure from 2023-07-04 with 360 s integration time, represented as amplitude ρ and absolute phase ϕ, plotted against spatial frequency. The color scheme encodes the corresponding baseline of the VLTI for two linear polarizations, each with nine spectral channels. The solid lines depict the model as reconstructed from a total of 16 exposures.

B.2 Fitting of GRAVITY data

Besides imaging with G$^{\mathrm{R}}$, we apply two other tools to analyze GRAVITY data. These methods serve to fit individual stars, that is, parameterized point sources, foremost to determine their astrometry and photometry. They allow for a crucial cross-check if S301 is inferred at the same position with a comparable photometry as with image reconstruction. Both fitting approaches are separately implemented in different programming languages.

In a first step, every GRAVITY exposure is fit separately to infer the variable flux of Sgr A*, equivalent to determining a light curve over time. Both inferred fluxes and positions of Sgr A* and other bright, known sources then provide the starting value for a subsequent combined fit. S301 is indeed inferred by both methods at the same position as with imaging, within statistical errors.

While the fitting codes yield the same positions for S301 as G$^{\mathrm{R}}$, it would be de facto impossible to find a star like S301 using just a fitting code. The fitting essentially returns a local minimum, while the imaging efficiently explores the full parameter space.

B.3 Astrometric errors

Errors in astrometry derived from images generally suffer from a bias due to the pixel grid. If the same faint source is inferred in the same pixel for the ten individual runs, the corresponding standard deviation is zero, albeit unphysical. Hence, the discretized position space needs to be considered when stating errors on astrometry. Instead of quantifying the error based on the number of same-pixel inferences in a set of detections, we opt for a general approach, which may be conservative, but prevents an underestimation of errors. We derive a discretization error by calculating the root mean square error for a single pixel within the image for both directions, RA. and

Dec., independently. Considering a pixel size of 0.8 mas per pixel, this evaluates to $\approx 207\,\mu$as and represents the statistical uncertainty in astrometry originating from the pixel grid in G^R images.

Appendix C Best-fit orbit

We fit the astrometric positions of S301 as in [11], taking into account Rømer delay and the 1PN correction of the motion due to the Schwarzschild nature of the gravitational potential. Relativistic Doppler effect and gravitational redshift do not matter as they only affect radial velocity measurements, which we currently don't have. This lack also results in a ambiguity in the three-dimensional orientation of the orbit. The two viable orbit solutions to the proper motion of S301 are given in Table C2 (angle conventions follow [19]) and leave the semi-major axis, eccentricity, and time of periastron unchanged within errors. In principle, the Rømer delay could break the ambiguity [20], but does not yet for the limited phase coverage of S301. The orbit stands out compared to other S-stars. For an illustration see figure C2 and D3, left. S301's high eccentricity, combined with the small value of the semi-major axis makes S301 an outlier with the smallest value of $r_p = a(1-e)$. Also note that the orbital plane of one of the two possible solutions agrees to within 3° with the inner clockwise disk of young, massive stars in [45].

Table C2 Best-fit orbit parameters for S301. The two sets give the two possible orbit orientations.

Parameter	Value	formal fit error	Value	formal fit error
a [mas]	83.0	0.4	83.0	0.5
e	0.9825	0.0013	0.9816	0.0006
i [°]	123.278	0.82	121.98	0.26
Ω [°]	76.0	2.7	259.07	0.40
ω [°]	294.7	1.9	116.36	0.55
t_P [yr]	2023.119	0.0095	2023.117	0.002
P [yr]	8.69	0.06	8.69	0.08
χ^2	29.065		29.057	

Appendix D Mass and age of S301

We infer the possible ages and masses of this star, using the observed brightness and the MIST [47–49] isochrones[1]. Specifically, we identify evolutionary points where the track magnitude crosses the inferred absolute magnitude. The stellar ages and masses for such points are shown as a solid, blue line in Fig. D3 (right). Note that the MIST tracks do not include the K band magnitude, and we use the JWST F210M magnitude as a proxy.

To test the robustness of our results we repeat this analysis with the K band magnitude from PARSEC isochrones (v1.2S, [50–54]), and show the possible ages

[1] MIST Version 1.2 tracks with $\Omega/\Omega_{\rm crit} = 0.4$ and solar metallicity

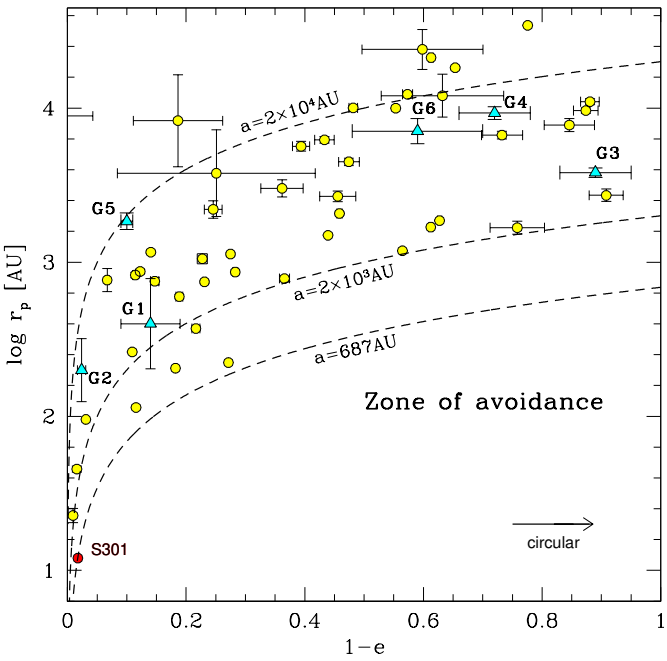

Fig. C2 Pericenter distance r_p versus $(1-e)$, with e the eccentricity of S-stars (yellow points) and G-clouds (cyan triangles) orbiting the central MBH [42, 46]. The dashed lines connect points of constant a. The orbits of all stars in the lower right, empty region should have been determined by now. The lack of stars in this so-called 'zone of avoidance' results from the fact that no stars exist in this regime because of a correlation between semi-major axis a and $(1-e)$, such that stars on more circular orbits with smaller values of e have larger semi-major axes. S301 is depicted by the red point in the lower left corner.

and masses as a dashed, orange line in Fig. D3. We note that unlike MIST, the PARSEC tracks do not include stellar rotation. Nonetheless the results are in excellent agreement, with the stellar mass ranging from $\sim 1.1 M_\odot$ to $\sim 1.5 M_\odot$, depending on the age of the star.

Appendix E Tidal effects

The energy input per orbit can be estimated, using the [55] formalism, viz.

$$\Delta E \approx T_2(\eta) \left(\frac{M_{\rm MBH}}{m_\star}\right)^2 \frac{G m_\star^2}{R_\star} \left(\frac{r_p}{R_\star}\right)^{-6}$$
$$\eta = \left(\frac{m_\star}{M_{\rm MBH}}\right)^{1/2} \left(\frac{r_p}{R_\star}\right)^{3/2}, \qquad \text{(E1)}$$

where r_p is the pericenter distance, $R_\star$ the stellar radius, $m_\star$ the stellar mass, and T_2 the tidal coupling constant. Here, we only include the leading order quadrupole term. We estimate the tidal coupling constant using the fits from [56], assuming an $n = 3$

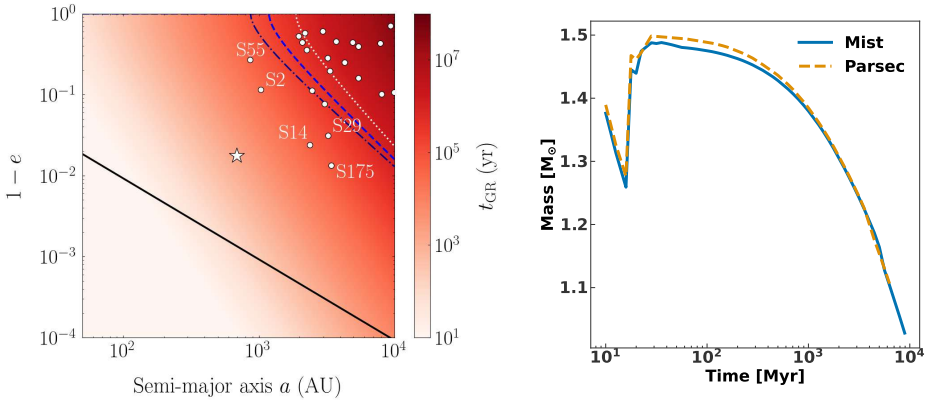

Fig. D3 Left: Dynamical landscape in the a versus $(1-e)$ phase space (in AU). The color map indicates $t_{\rm GR}$. The Schwarzschild Barrier (SB) boundary ($t_{\rm GR} = t_{{\rm RR},v}$) shifts significantly depending on the cusp slope γ. Boundaries are shown for the observed shallow cusp ($\gamma = 1.3$, dotted curve) and steep theoretical cusps ($\gamma = 1.75$, dashed curve; $\gamma = 2.0$, dash-dotted curve), assuming normalization at 0.25 pc. S301 (white asterisk) and other young S-stars (white circles) remain deep within the barrier in all scenarios. The solid line indicates the tidal disruption limit for S301 ($1.5\,M_\odot, 1.4\,R_\odot$). Right: Locus of possible ages and masses for S301, from its observed K-band magnitude and theoretical isochrones.

polytrope. Note that these fits only extend to $\eta = 10$, and we extrapolate them using the logarithmic slope there. Thus,

$$T(\eta) \approx 3.8 \times 10^{-5} \left(\frac{\eta}{10}\right)^{-6.5} \tag{E2}$$

for $\eta \geq 10$. Thus, $\delta E \approx 10^{-16} G m_\star^2 / R_\star$. It would take of order 10^{17} yr for tides to inject an order unity fraction of the energy of the star. Therefore, tidal heating can be neglected at the star's current orbit.

Appendix F Comparison with previously claimed short-period stars

Over the past five year, a number of short-period stars with orbital periods as low as 4 years were claimed to have been discovered by one team using adaptive-optics based imaging techniques [57–59], thus at a resolution 15 times worse than the GRAVITY data. Safely, we can exclude that the objects in [57] named S4711 and S62 (different from the star our team calls S62, see [60]), and that have similar orbital periods as S301, are actually S301:

- The eccentricity of S4711 with $e = 0.768$ is considerably less than S301's, and the claimed orbit has a different projection on sky, extending towards the East.
- While S62 features a comparable eccentricity of $e = 0.976$, the claimed orbit revolves counter-clockwise, unlike S301.

Beyond that, none of the other claimed stars have orbital elements similar to the ones of S301. Hence, S301 is newly discovered.

Further it is worth noting that the limiting magnitude of $m_K \sim 20$ inferred from the GRAVITY observations and reported here should have allowed us to easily detect any of the claimed discoveries if covered in our exposures. In none of our reconstructed images we have detected a significant contribution of flux beyond background noise that one could attribute to the claimed stars.

Appendix G Newtonian perturbations of the spin measurement

The simulations for the spin measurement assume that S301 orbits an isolated Kerr black hole in the absence of external perturbations. As noted by [28], gravitational perturbations from a population of stellar-mass black holes, expected to form a power-law-density stellar cusp around Sgr A*, can induce orbital precession comparable in magnitude to the Lense-Thirring effect, thereby complicating the measurement of the spin. Recent constraints from [61] limit the extended mass within the central 10 mpc to $\lesssim 1200\,M_\odot$. To assess the impact of a realistic perturber population, following [62] we performed N-body simulations of S301 including a cluster of 60 stellar-mass black holes of $20\,M_\odot$ each, distributed within 10 mpc of Sgr A* according to a density profile $\rho(r) \propto r^{-2}$. Considering 100 independent realizations of the initial conditions, we find that the cluster induces an average orbital-plane precession per orbital period of $0.65^{+0.36}_{-0.56}$ arcminutes. This contribution is typically subdominant compared to the Lense-Thirring precession for moderate-to-high dimensionless spins and favorable orientations of the black-hole spin relative to the orbital angular momentum. Importantly, the Lense-Thirring effect is concentrated near pericenter, whereas perturbations from a granular stellar background tend to produce their largest observable deviations near apocenter [62, 63]. This phase separation, together with the distinct temporal signatures of the two effects, offers a promising avenue to disentangle the relativistic spin signal from stellar perturbations and thereby enable a robust measurement of the MBH spin.

Appendix H Dynamical time scales for S301

In this section we will estimate the times cales for the orbital relaxation and collisions for S301.

H.1 Relaxation times

Relaxation is the dynamical evolution of objects due to perturbations from their environment. In the Galactic Center relaxation can be subdivided into resonant and non-resonant parts. Resonant relaxation corresponds to the evolution of stellar orbits due to coherent torques from the background. This can lead to rapid evolution of angular momentum. On longer times cales, non-resonant (two-body) relaxation evolves the orbital energy due to uncorrelated two-body encounters. (See [64] for a review)

The two-body relaxation time scale is approximately (see equation 5.61 in [65])

$$t_{rx} = 0.34 \frac{\sigma^3}{G^2 n \langle m^2 \rangle \ln \Lambda} \tag{H3}$$

where $\sigma \approx \sqrt{GM/(1+\gamma)/r}$ is the (1D) velocity dispersion, n is the number density (with power-law index $-\gamma$). $\langle m^2 \rangle$ is the second moment of the mass function. Due to the quadratic mass dependence, the most massive species (viz. stellar mass black holes) often dictate this time scale.

We follow [66] to estimate the background density profile. We model the background as two species: 10 $M_\odot$ black holes and 1 $M_\odot$ stars. This is a reasonable approximation for modeling relaxation in an evolved galactic nucleus, and has been used extensively in the literature [65]. The stars are initialized with a Nuker density profile [67], viz.

$$\rho_o \left(\frac{r}{r_o}\right)^{-\gamma} \left[1 + \left(\frac{r}{r_o}\right)^{\alpha}\right]^{(\gamma-\beta)/\alpha}, \tag{H4}$$

with γ=1.5, α=2, and β=5. The density normalization is set by the total mass: $2.5 \times 10^7 M_\odot$ and $2.5 \times 10^5 M_\odot$ for the stars and black holes respectively. The central MBH starts at $4.15 \times 10^6 M_\odot$ and grows to $4.27 \times 10^6 M_\odot$ by consuming stars and black holes. The profile is allowed to relax for 10 Gyr, such that the final density profiles are not too sensitive to the initial conditions. In the end the total mass within 0.01 pc is approximately $1200 M_\odot$, consistent with the latest constraints on the enclosed mass within S2's apocentre [61]. Furthermore the final stellar density at 1 pc ($\approx 9 \times 10^4 M_\odot$ pc^{-3}) is comparable to observational estimates [68].

The following power-law fits approximate the final density profile between $\sim 10^{-4}$ and 0.01 pc

$$\begin{aligned}
\rho_{\rm bh} &= 4.95 \times 10^8 \left(\frac{r}{0.0033\,{\rm pc}}\right)^{-1.75} M_\odot\,{\rm pc}^{-3} \\
\rho_* &= 3.46 \times 10^8 \left(\frac{r}{0.0033\,{\rm pc}}\right)^{-1.4} M_\odot\,{\rm pc}^{-3},
\end{aligned} \tag{H5}$$

Combining equations (H3) and (H5) we find that the two-body relaxation time scale at S301's semi-major axis (3.3×10^{-3} pc) would be $\sim 9 \times 10^8$ yr.

To estimate the angular momentum relaxation time, including resonant relaxation, we follow [69] (and the references therein). In particular we use their software, JuDOKA[2], to compute diffusion coefficients ($D_{\rm jj}$) as a function of eccentricity and semi-major axis for the density profiles in eq. (H5).

The angular momentum relaxation times can then be estimated using

$$t_{\rm rx,j(NRR)} = \frac{j^2}{D_{\rm jj,NRR}}$$

[2] https://github.com/KerwannTEP/JuDOKA

$$t_{\mathrm{rx,j(RR)}} = \frac{j^2}{D_{\mathrm{jj,NRR}} + D_{\mathrm{jj,RR}}}, \tag{H6}$$

where j is the angular momentum normalized to the circular angular momentum at the same energy. The top (bottom) row corresponds to the time scale without (with) resonant relaxation. We find that both $t_{\mathrm{rx,j(NRR)}}$ and $t_{\mathrm{rx,j(RR)}}$ are $\approx 3 \times 10^7$ yr for S301, indicating that resonant relaxation is unimportant for this star. This is expected, because of the star's short Schwarzschild-precession time scale. In other words, the star lies within the Schwarzschild barrier, where rapid precession suppresses the build-up of coherent torques [e.g. 70].

Alternatively, $t_{\mathrm{rx,j(NRR)}} \approx j^2 t_{\mathrm{rx}}$, which gives results that are consistent with equation (H3).

H.2 Collision time scales

The mean time between collisions for a single target star is

$$t_{\mathrm{coll}} = \frac{1}{n\,\Sigma\,v_{\mathrm{rel}}}, \tag{H7}$$

where n is the local number density of potential impactors, v_{rel} is the typical relative velocity, and Σ is the collisional cross section. For a star of radius $R_\star$ and mass $m_\star$ colliding with objects of mass m_{imp} and radius R_{imp}, the cross section including gravitational focusing is

$$\Sigma = \pi\,(R_\star + R_{\mathrm{imp}})^2 \left(1 + \frac{v_{\mathrm{esc}}^2}{v_{\mathrm{rel}}^2}\right), \qquad v_{\mathrm{esc}}^2 = \frac{2G\,(m_\star + m_{\mathrm{imp}})}{(R_\star + R_{\mathrm{imp}})}. \tag{H8}$$

In the case of S301, $m_\star \approx 1.5 M_\odot$ and $R_\star \approx 1.4 R_\odot$. Then from eq. (H5) and (H8) the local collision time scale would be $\sim 2.0 \times 10^9$ yr for stellar mass black holes and $\sim 2.1 \times 10^8$ yr for stars.

H.3 Uncertainties, caveats and other effects

The relaxation and collision time scales we estimate above are local. In principle, the interactions at pericenter can significantly shorten the energy relaxation and collision time scales. A naive orbit average with the background profile in equation (H5), would suggest a reduction at the order of magnitude level. In practice, fewer than one scatterer is expected at S301's pericenter for our assumed density profiles, so the local time scales are more realistic.

Our time scale estimates implicitly assume stars are evolving through a localized diffusion process. In reality, angular momentum and energy perturbations from a handful of massive perturbers exhibit a heavy power-law tail, such that orbital evolution would be dominated by large, non-local jumps that can speed up the orbital evolution dramatically [71].

References

[1] Blandford, R., Meier, D., Readhead, A.: Relativistic Jets from Active Galactic Nuclei. ARA&A **57**, 467–509 (2019) https://doi.org/10.1146/annurev-astro-081817-051948 arXiv:1812.06025 [astro-ph.HE]

[2] Tanaka, Y., Nandra, K., Fabian, A.C., Inoue, H., Otani, C., Dotani, T., Hayashida, K., Iwasawa, K., Kii, T., Kunieda, H., Makino, F., Matsuoka, M.: Gravitationally redshifted emission implying an accretion disk and massive black hole in the active galaxy MCG-6-30-15. Nature **375**, 659–661 (1995) https://doi.org/10.1038/375659a0

[3] McClintock, J.E., Shafee, R., Narayan, R., Remillard, R.A., Davis, S.W., Li, L.-X.: The Spin of the Near-Extreme Kerr Black Hole GRS 1915+105. ApJ **652**(1), 518–539 (2006) https://doi.org/10.1086/508457 arXiv:astro-ph/0606076 [astro-ph]

[4] Abbott, B.P., Abbott, R., Abbott, T.D., Abernathy, M.R., Acernese, F., Ackley, K., Adams, C., Adams, T., Addesso, P., Adhikari, R.X., al.: GW151226: Observation of Gravitational Waves from a 22-Solar-Mass Binary Black Hole Coalescence. Physical Review Letters **116**(24), 241103 (2016) https://doi.org/10.1103/PhysRevLett.116.241103 arXiv:1606.04855 [gr-qc]

[5] Collaboration, L.S., Collaboration, V., Collaboration, K.: Black hole spectroscopy and tests of general relativity with gw250114. arXiv e-prints (2025) arXiv:2509.08099 [gr-qc]

[6] Everitt, C.W.F., Debra, D.B., Parkinson, B.W., Turneaure, J.P., Conklin, J.W., Heifetz, M.I., Keiser, G.M., Silbergleit, A.S., Holmes, T., Kolodziejczak, J., Al-Meshari, M., Mester, J.C., Muhlfelder, B., Solomonik, V.G., Stahl, K., Worden, P.W. Jr., Bencze, W., Buchman, S., Clarke, B., Al-Jadaan, A., Al-Jibreen, H., Li, J., Lipa, J.A., Lockhart, J.M., Al-Suwaidan, B., Taber, M., Wang, S.: Gravity Probe B: Final Results of a Space Experiment to Test General Relativity. Phys. Rev. Lett. **106**(22), 221101 (2011) https://doi.org/10.1103/PhysRevLett.106.221101 arXiv:1105.3456 [gr-qc]

[7] Adler, R.J.: The three-fold theoretical basis of the gravity probe b gyro precession calculation. Classical and Quantum Gravity **32**(22), 224002 (2015) https://doi.org/10.1088/0264-9381/32/22/224002

[8] Genzel, R.: A Forty Year Journey. arXiv e-prints, 2102–13000 (2021) https://doi.org/10.48550/arXiv.2102.13000 arXiv:2102.13000 [astro-ph.GA]

[9] Schdel, R., Ott, T., Genzel, R., Hofmann, R., Lehnert, M., Eckart, A., Mouawad, N., Alexander, T., Reid, M.J., Lenzen, R., Hartung, M., Lacombe, F., Rouan, D., Gendron, E., Rousset, G., Lagrange, A.-M., Brandner, W., Ageorges, N., Lidman, C., Moorwood, A.F.M., Spyromilio, J., Hubin, N., Menten, K.M.: A star in a

15.2-year orbit around the supermassive black hole at the centre of the Milky Way. Nature **419**(6908), 694–696 (2002) https://doi.org/10.1038/nature01121 . Publisher: Nature Publishing Group

[10] Gravity Collaboration, Abuter, R., Amorim, A., Anugu, N., Bauböck, M., Benisty, M., Berger, J.P., Blind, N., Bonnet, H., Brandner, W., Buron, A., Collin, C., Chapron, F., Clénet, Y., Coudé Du Foresto, V., de Zeeuw, P.T., Deen, C., Delplancke-Ströbele, F., Dembet, R., Dexter, J., Duvert, G., Eckart, A., Eisenhauer, F., Finger, G., Förster Schreiber, N.M., Fédou, P., Garcia, P., Garcia Lopez, R., Gao, F., Gendron, E., Genzel, R., Gillessen, S., Gordo, P., Habibi, M., Haubois, X., Haug, M., Haußmann, F., Henning, T., Hippler, S., Horrobin, M., Hubert, Z., Hubin, N., Jimenez Rosales, A., Jochum, L., Jocou, K., Kaufer, A., Kellner, S., Kendrew, S., Kervella, P., Kok, Y., Kulas, M., Lacour, S., Lapeyrère, V., Lazareff, B., Le Bouquin, J.-B., Léna, P., Lippa, M., Lenzen, R., Mérand, A., Müler, E., Neumann, U., Ott, T., Palanca, L., Paumard, T., Pasquini, L., Perraut, K., Perrin, G., Pfuhl, O., Plewa, P.M., Rabien, S., Ramírez, A., Ramos, J., Rau, C., Rodríguez-Coira, G., Rohloff, R.-R., Rousset, G., Sanchez-Bermudez, J., Scheithauer, S., Schöller, M., Schuler, N., Spyromilio, J., Straub, O., Straubmeier, C., Sturm, E., Tacconi, L.J., Tristram, K.R.W., Vincent, F., von Fellenberg, S., Wank, I., Waisberg, I., Widmann, F., Wieprecht, E., Wiest, M., Wiezorrek, E., Woillez, J., Yazici, S., Ziegler, D., Zins, G.: Detection of the gravitational redshift in the orbit of the star S2 near the Galactic centre massive black hole. A&A **615**, 15 (2018) https://doi.org/10.1051/0004-6361/201833718 arXiv:1807.09409

[11] Gravity Collaboration, Abuter, R., Amorim, A., Bauböck, M., Berger, J.P., Bonnet, H., Brandner, W., Cardoso, V., Clénet, Y., de Zeeuw, P.T., Dexter, J., Eckart, A., Eisenhauer, F., Förster Schreiber, N.M., Garcia, P., Gao, F., Gendron, E., Genzel, R., Gillessen, S., Habibi, M., Haubois, X., Henning, T., Hippler, S., Horrobin, M., Jiménez-Rosales, A., Jochum, L., Jocou, L., Kaufer, A., Kervella, P., Lacour, S., Lapeyrère, V., Le Bouquin, J.-B., Léna, P., Nowak, M., Ott, T., Paumard, T., Perraut, K., Perrin, G., Pfuhl, O., Rodríguez-Coira, G., Shangguan, J., Scheithauer, S., Stadler, J., Straub, O., Straubmeier, C., Sturm, E., Tacconi, L.J., Vincent, F., von Fellenberg, S., Waisberg, I., Widmann, F., Wieprecht, E., Wiezorrek, E., Woillez, J., Yazici, S., Zins, G.: Detection of the Schwarzschild precession in the orbit of the star S2 near the Galactic centre massive black hole. A&A **636**, 5 (2020) https://doi.org/10.1051/0004-6361/202037813 arXiv:2004.07187 [astro-ph.GA]

[12] GRAVITY Collaboration, Abuter, R., Aimar, N., Amorim, A., Ball, J., Bauböck, M., Berger, J.P., Bonnet, H., Bourdarot, G., Brandner, W., Cardoso, V., Clénet, Y., Dallilar, Y., Davies, R., de Zeeuw, P.T., Dexter, J., Drescher, A., Eisenhauer, F., Förster Schreiber, N.M., Foschi, A., Garcia, P., Gao, F., Gendron, E., Genzel, R., Gillessen, S., Habibi, M., Haubois, X., Heißel, G., Henning, T., Hippler, S., Horrobin, M., Jochum, L., Jocou, L., Kaufer, A., Kervella, P., Lacour, S., Lapeyrère, V., Le Bouquin, J.-B., Léna, P., Lutz, D., Ott, T., Paumard, T.,

Perraut, K., Perrin, G., Pfuhl, O., Rabien, S., Shangguan, J., Shimizu, T., Scheithauer, S., Stadler, J., Stephens, A.W., Straub, O., Straubmeier, C., Sturm, E., Tacconi, L.J., Tristram, K.R.W., Vincent, F., von Fellenberg, S., Widmann, F., Wieprecht, E., Wiezorrek, E., Woillez, J., Yazici, S., Young, A.: Mass distribution in the Galactic Center based on interferometric astrometry of multiple stellar orbits. A&A **657**, 12 (2022) https://doi.org/10.1051/0004-6361/202142465 arXiv:2112.07478 [astro-ph.GA]

[13] Gravity Collaboration, Abuter, R., Accardo, M., Amorim, A., Anugu, N., Ávila, G., Azouaoui, N., Benisty, M., Berger, J.P., Blind, N., Bonnet, H., Bourget, P., Brandner, W., Brast, R., Buron, A., Burtscher, L., Cassaing, F., Chapron, F., Choquet, É., Clénet, Y., Collin, C., Coudé Du Foresto, V., de Wit, W., de Zeeuw, P.T., Deen, C., Delplancke-Ströbele, F., Dembet, R., Derie, F., Dexter, J., Duvert, G., Ebert, M., Eckart, A., Eisenhauer, F., Esselborn, M., Fédou, P., Finger, G., Garcia, P., Garcia Dabo, C.E., Garcia Lopez, R., Gendron, E., Genzel, R., Gillessen, S., Gonte, F., Gordo, P., Grould, M., Grözinger, U., Guieu, S., Haguenauer, P., Hans, O., Haubois, X., Haug, M., Haussmann, F., Henning, T., Hippler, S., Horrobin, M., Huber, A., Hubert, Z., Hubin, N., Hummel, C.A., Jakob, G., Janssen, A., Jochum, L., Jocou, L., Kaufer, A., Kellner, S., Kendrew, S., Kern, L., Kervella, P., Kiekebusch, M., Klein, R., Kok, Y., Kolb, J., Kulas, M., Lacour, S., Lapeyrère, V., Lazareff, B., Le Bouquin, J.-B., Lèna, P., Lenzen, R., Lévêque, S., Lippa, M., Magnard, Y., Mehrgan, L., Mellein, M., Mérand, A., Moreno-Ventas, J., Moulin, T., Müller, E., Müller, F., Neumann, U., Oberti, S., Ott, T., Pallanca, L., Panduro, J., Pasquini, L., Paumard, T., Percheron, I., Perraut, K., Perrin, G., Pflüger, A., Pfuhl, O., Phan Duc, T., Plewa, P.M., Popovic, D., Rabien, S., Ramírez, A., Ramos, J., Rau, C., Riquelme, M., Rohloff, R.-R., Rousset, G., Sanchez-Bermudez, J., Scheithauer, S., Schöller, M., Schuhler, N., Spyromilio, J., Straubmeier, C., Sturm, E., Suarez, M., Tristram, K.R.W., Ventura, N., Vincent, F., Waisberg, I., Wank, I., Weber, J., Wieprecht, E., Wiest, M., Wiezorrek, E., Wittkowski, M., Woillez, J., Wolff, B., Yazici, S., Ziegler, D., Zins, G.: First light for GRAVITY: Phase referencing optical interferometry for the Very Large Telescope Interferometer. A&A **602**, 94 (2017) https://doi.org/10.1051/0004-6361/201730838 arXiv:1705.02345 [astro-ph.IM]

[14] Lense, J., Thirring, H.: Ueber den Einfluss der Eigenrotation der Zentralkoerper auf die Bewegung der Planeten und Monde nach der Einsteinschen Gravitationstheorie. Phys. Z. **19**, 156–163 (1918)

[15] Waisberg, I., Dexter, J., Gillessen, S., Pfuhl, O., Eisenhauer, F., Plewa, P.M., Bauböck, M., Jimenez-Rosales, A., Habibi, M., Ott, T., von Fellenberg, S., Gao, F., Widmann, F., Genzel, R.: What stellar orbit is needed to measure the spin of the Galactic centre black hole from astrometric data? MNRAS **476**(3), 3600–3610 (2018) https://doi.org/10.1093/mnras/sty476 arXiv:1802.08198 [astro-ph.GA]

[16] Hills, J.G.: Hyper-velocity and tidal stars from binaries disrupted by a massive Galactic black hole. Nature **331**, 687 (1988) https://doi.org/10.1038/331687a0 .

Publisher: Nature Publishing Group

[17] GRAVITY Collaboration, Abuter, R., Aimar, N., Amorim, A., Arras, P., Baubck, M., Berger, J.P., Bonnet, H., Brandner, W., Bourdarot, G., Cardoso, V., Clnet, Y., Davies, R., De Zeeuw, P.T., Dexter, J., Dallilar, Y., Drescher, A., Eisenhauer, F., Enlin, T., Frster Schreiber, N.M., Garcia, P., Gao, F., Gendron, E., Genzel, R., Gillessen, S., Habibi, M., Haubois, X., Heiel, G., Henning, T., Hippler, S., Horrobin, M., Jimnez-Rosales, A., Jochum, L., Jocou, L., Kaufer, A., Kervella, P., Lacour, S., Lapeyrre, V., Le Bouquin, J.-B., Lna, P., Lutz, D., Mang, F., Nowak, M., Ott, T., Paumard, T., Perraut, K., Perrin, G., Pfuhl, O., Rabien, S., Shangguan, J., Shimizu, T., Scheithauer, S., Stadler, J., Straub, O., Straubmeier, C., Sturm, E., Tacconi, L.J., Tristram, K.R.W., Vincent, F., Von Fellenberg, S., Waisberg, I., Widmann, F., Wieprecht, E., Wiezorrek, E., Woillez, J., Yazici, S., Young, A., Zins, G.: Deep images of the Galactic center with GRAVITY. Astronomy & Astrophysics **657**, 82 (2022) https://doi.org/10.1051/0004-6361/202142459

[18] Mang, F., et al.: GRAVITY-RESOLVE: A comprehensive image reconstruction tool for Galactic Center observations with GRAVITY. Article in prep. (2026)

[19] Gillessen, S., Eisenhauer, F., Trippe, S., Alexander, T., Genzel, R., Martins, F., Ott, T.: Monitoring Stellar Orbits Around the Massive Black Hole in the Galactic Center. ApJ **692**(2), 1075–1109 (2009) https://doi.org/10.1088/0004-637X/692/2/1075 arXiv:0810.4674 [astro-ph]

[20] Abuter, R., Amorim, A., Baubck, M., Berger, J.P., Bonnet, H., Brandner, W., Clnet, Y., Foresto, V.C.d., Zeeuw, P.T.d., Dexter, J., Duvert, G., Eckart, A., Eisenhauer, F., Schreiber, N.M.F., Garcia, P., Gao, F., Gendron, E., Genzel, R., Gerhard, O., Gillessen, S., Habibi, M., Haubois, X., Henning, T., Hippler, S., Horrobin, M., Jimnez-Rosales, A., Jocou, L., Kervella, P., Lacour, S., Lapeyrre, V., Bouquin, J.-B.L., Lna, P., Ott, T., Paumard, T., Perraut, K., Perrin, G., Pfuhl, O., Rabien, S., Coira, G.R., Rousset, G., Scheithauer, S., Sternberg, A., Straub, O., Straubmeier, C., Sturm, E., Tacconi, L.J., Vincent, F., Fellenberg, S.v., Waisberg, I., Widmann, F., Wieprecht, E., Wiezorrek, E., Woillez, J., Yazici, S.: A geometric distance measurement to the Galactic center black hole with 0.3% uncertainty. Astronomy & Astrophysics **625**, 10 (2019) https://doi.org/10.1051/0004-6361/201935656 . Publisher: EDP Sciences

[21] Meyer, L., Ghez, A., Schödel, R., Yelda, S., Boehle, A., Lu, J.R., Do, T., Morris, M.R., Becklin, E.E., Matthews, K.: The Shortest-Known-Period Star Orbiting Our Galaxy's Supermassive Black Hole. Science **338**(6), 84–87 (2012)

[22] Fritz, T.K., Gillessen, S., Dodds-Eden, K., Lutz, D., Genzel, R., Raab, W., Ott, T., Pfuhl, O., Eisenhauer, F., Yusef-Zadeh, F.: Line Derived Infrared Extinction toward the Galactic Center. ApJ **737**(2), 73 (2011) https://doi.org/10.1088/0004-637X/737/2/73 arXiv:1105.2822 [astro-ph.GA]

[23] Genzel, R., Eisenhauer, F., Gillessen, S.: The Galactic Center massive black hole and nuclear star cluster. Rev. Mod. Phys. **82**(4), 3121–3195 (2010)

[24] Cox, A.: Allen's Astrophysical Quantities. AIP, New York, NY (2000). https://doi.org/10.1007/978-1-4612-1186-0 . https://cds.cern.ch/record/441599

[25] Hanson, M.M., Conti, P.S., Rieke, M.J.: A Spectral Atlas of Hot, Luminous Stars at 2 Microns. ApJS **107**, 281 (1996) https://doi.org/10.1086/192366

[26] Davies, R., Hörmann, V., Rabien, S., Sturm, E., Alves, J., Clénet, Y., Kotilainen, J., Lang-Bardl, F., Nicklas, H., Pott, J.-U., Tolstoy, E., Vulcani, B., MICADO Consortium: MICADO: The Multi-Adaptive Optics Camera for Deep Observations. The Messenger **182**, 17–21 (2021) https://doi.org/10.18727/0722-6691/5217 arXiv:2103.11631 [astro-ph.IM]

[27] Psaltis, D., Li, G., Loeb, A.: Deviation of Stellar Orbits from Test Particle Trajectories around Sgr A* Due to Tides and Winds. ApJ **777**(1), 57 (2013) https://doi.org/10.1088/0004-637X/777/1/57 arXiv:1212.3342 [astro-ph.HE]

[28] Merritt, D., Alexander, T., Mikkola, S., Will, C.M.: Testing properties of the Galactic center black hole using stellar orbits. Phys. Rev. D **81**(6), 062002 (2010) https://doi.org/10.1103/PhysRevD.81.062002 arXiv:0911.4718 [astro-ph.GA]

[29] El Dayem, K.A., Vincent, F.H., Heissel, G., Paumard, T., Perrin, G.: The effects of the spin and quadrupole moment of SgrA* on the orbits of S stars. arXiv e-prints, 2505–24789 (2025) https://doi.org/10.48550/arXiv.2505.24789 arXiv:2505.24789 [astro-ph.GA]

[30] Levin, Y., Beloborodov, A.M.: Stellar Disk in the Galactic Center: A Remnant of a Dense Accretion Disk? ApJ **590**(1), 33–36 (2003) https://doi.org/10.1086/376675 arXiv:astro-ph/0303436 [astro-ph]

[31] Abd El Dayem, K., et al.: Detectability of the spin parameters of SgrA* using multiple S stars. Article in prep. (2026)

[32] Will, C.M.: Testing the General Relativistic "No-Hair" Theorems Using the Galactic Center Black Hole Sagittarius A*. ApJ **674**(1), 25 (2008) https://doi.org/10.1086/528847 arXiv:0711.1677 [astro-ph]

[33] Kocsis, B., Tremaine, S.: Resonant relaxation and the warp of the stellar disc in the Galactic Centre. MNRAS **412**(1), 187–207 (2011) https://doi.org/10.1111/j.1365-2966.2010.17897.x arXiv:1006.0001 [astro-ph.GA]

[34] Peters, P.C.: Gravitational radiation and the motion of two point masses. Physical Review **136**, 1224–1232 (1964) https://doi.org/10.1103/PhysRev.136.B1224

[35] Press, W.H., Teukolsky, S.A.: On the destruction of stars by neutron stars and

black holes. Astrophysical Journal **213**, 183–192 (1977) https://doi.org/10.1086/155148

[36] Yu, Q., Tremaine, S.: Ejection of Hypervelocity Stars by the (Binary) Black Hole in the Galactic Center. ApJ **599**(2), 1129–1138 (2003) https://doi.org/10.1086/379546 arXiv:astro-ph/0309084 [astro-ph]

[37] Gould, A., Quillen, A.C.: Sagittarius A* Companion S0-2: A Probe of Very High Mass Star Formation. ApJ **592**(2), 935–940 (2003) https://doi.org/10.1086/375840 arXiv:astro-ph/0302437 [astro-ph]

[38] Ginsburg, I., Loeb, A.: The fate of former companions to hypervelocity stars originating at the Galactic Centre. MNRAS **368**(1), 221–225 (2006) https://doi.org/10.1111/j.1365-2966.2006.10091.x arXiv:astro-ph/0510574 [astro-ph]

[39] Perets, H.B., Hopman, C., Alexander, T.: Massive Perturber-driven Interactions between Stars and a Massive Black Hole. ApJ **656**(2), 709–720 (2007) https://doi.org/10.1086/510377 arXiv:astro-ph/0606443 [astro-ph]

[40] Generozov, A., Madigan, A.-M.: The Hills Mechanism and the Galactic Center S-stars. ApJ **896**(2), 137 (2020) https://doi.org/10.3847/1538-4357/ab94bc arXiv:2002.10547 [astro-ph.GA]

[41] Hills, J.G.: Computer Simulations of Encounters Between Massive Black Holes and Binaries. AJ **102**, 704 (1991) https://doi.org/10.1086/115905

[42] Generozov, A., Perets, H.B., Bordoni, M.S., Bourdarot, G., Drescher, A., Eisenhauer, F., Genzel, R., Gillessen, S., Mang, F., Ott, T., Ribeiro, D.C., Schödel, R.: The S stars' zone of avoidance in the Galactic center. A&A **696**, 68 (2025) https://doi.org/10.1051/0004-6361/202453272 arXiv:2412.02752 [astro-ph.GA]

[43] Raghavan, D., McAlister, H.A., Henry, T.J., Latham, D.W., Marcy, G.W., Mason, B.D., Gies, D.R., White, R.J., ten Brummelaar, T.A.: A Survey of Stellar Families: Multiplicity of Solar-type Stars. ApJS **190**(1), 1–42 (2010) https://doi.org/10.1088/0067-0049/190/1/1 arXiv:1007.0414 [astro-ph.SR]

[44] Brown, W.R.: Hypervelocity Stars. ARA&A **53**, 15–49 (2015) https://doi.org/10.1146/annurev-astro-082214-122230

[45] von Fellenberg, S.D., Gillessen, S., Stadler, J., Bauböck, M., Genzel, R., de Zeeuw, T., Pfuhl, O., Amaro Seoane, P., Drescher, A., Eisenhauer, F., Habibi, M., Ott, T., Widmann, F., Young, A.: The Young Stars in the Galactic Center. ApJ **932**(1), 6 (2022) https://doi.org/10.3847/2041-8213/ac68ef arXiv:2205.07595 [astro-ph.GA]

[46] Burkert, A., Gillessen, S., Lin, D.N.C., Zheng, X., Schoeller, P., Eisenhauer, F.,

Genzel, R.: The Orbital Structure and Selection Effects of the Galactic Center S-star Cluster. ApJ **962**(1), 81 (2024) https://doi.org/10.3847/1538-4357/ad17bb arXiv:2306.02076 [astro-ph.GA]

[47] Dotter, A.: MESA Isochrones and Stellar Tracks (MIST) 0: Methods for the Construction of Stellar Isochrones. ApJS **222**(1), 8 (2016) https://doi.org/10.3847/0067-0049/222/1/8 arXiv:1601.05144 [astro-ph.SR]

[48] Choi, J., Dotter, A., Conroy, C., Cantiello, M., Paxton, B., Johnson, B.D.: Mesa Isochrones and Stellar Tracks (MIST). I. Solar-scaled Models. ApJ **823**(2), 102 (2016) https://doi.org/10.3847/0004-637X/823/2/102 arXiv:1604.08592 [astro-ph.SR]

[49] Paxton, B., Marchant, P., Schwab, J., Bauer, E.B., Bildsten, L., Cantiello, M., Dessart, L., Farmer, R., Hu, H., Langer, N., Townsend, R.H.D., Townsley, D.M., Timmes, F.X.: Modules for Experiments in Stellar Astrophysics (MESA): Binaries, Pulsations, and Explosions. ApJS **220**, 15 (2015) https://doi.org/10.1088/0067-0049/220/1/15 arXiv:1506.03146 [astro-ph.SR]

[50] Bressan, A., Marigo, P., Girardi, L., Salasnich, B., Dal Cero, C., Rubele, S., Nanni, A.: PARSEC: stellar tracks and isochrones with the PAdova and TRieste Stellar Evolution Code. MNRAS **427**(1), 127–145 (2012) https://doi.org/10.1111/j.1365-2966.2012.21948.x arXiv:1208.4498 [astro-ph.SR]

[51] Chen, Y., Bressan, A., Girardi, L., Marigo, P., Kong, X., Lanza, A.: parsec evolutionary tracks of massive stars up to 350 $M_{\odot}$ at metallicities 0.0001 $\leq$ Z $\leq$ 0.04. Monthly Notices of the Royal Astronomical Society **452**(1), 1068–1080 (2015) https://doi.org/10.1093/mnras/stv1281 https://academic.oup.com/mnras/article-pdf/452/1/1068/4920265/stv1281.pdf

[52] Tang, J., Bressan, A., Rosenfield, P., Slemer, A., Marigo, P., Girardi, L., Bianchi, L.: New PARSEC evolutionary tracks of massive stars at low metallicity: testing canonical stellar evolution in nearby star-forming dwarf galaxies. Monthly Notices of the Royal Astronomical Society **445**(4), 4287–4305 (2014) https://doi.org/10.1093/mnras/stu2029 https://academic.oup.com/mnras/article-pdf/445/4/4287/6097104/stu2029.pdf

[53] Marigo, P., Girardi, L., Bressan, A., Rosenfield, P., Aringer, B., Chen, Y., Dussin, M., Nanni, A., Pastorelli, G., Rodrigues, T.S., Trabucchi, M., Bladh, S., Dalcanton, J., Groenewegen, M.A.T., Montalbán, J., Wood, P.R.: A New Generation of PARSEC-COLIBRI Stellar Isochrones Including the TP-AGB Phase. ApJ **835**(1), 77 (2017) https://doi.org/10.3847/1538-4357/835/1/77 arXiv:1701.08510 [astro-ph.SR]

[54] Pastorelli, G., Marigo, P., Girardi, L., Aringer, B., Chen, Y., Rubele, S., Trabucchi, M., Bladh, S., Boyer, M.L., Bressan, A., Dalcanton, J.J., Groenewegen, M.A.T., Lebzelter, T., Mowlavi, N., Chubb, K.L., Cioni, M.-R.L., de Grijs, R.,

Ivanov, V.D., Nanni, A., van Loon, J.T., Zaggia, S.: Constraining the thermally pulsing asymptotic giant branch phase with resolved stellar populations in the Large Magellanic Cloud. MNRAS **498**(3), 3283–3301 (2020) https://doi.org/10.1093/mnras/staa2565 arXiv:2008.08595 [astro-ph.SR]

[55] Press, W.H., Teukolsky, S.A.: On formation of close binaries by two-body tidal capture. ApJ **213**, 183–192 (1977) https://doi.org/10.1086/155143

[56] Portegies Zwart, S.F., Meinen, A.T.: Quick method for calculating energy dissipation in tidal interaction. A&A **280**(1), 174–176 (1993)

[57] Peiker, F., Eckart, A., Zajaek, M., Ali, B., Parsa, M.: S62 and S4711: Indications of a Population of Faint Fast-moving Stars inside the S2 OrbitS4711 on a 7.6 yr Orbit around Sgr A*. The Astrophysical Journal **899**(1), 50 (2020) https://doi.org/10.3847/1538-4357/ab9c1c . Publisher: The American Astronomical Society

[58] Peiker, F., Eckart, A., Zajaek, M., Ali, B., Parsa, M.: S62 and S4711: Indications of a Population of Faint Fast-moving Stars inside the S2 OrbitS4711 on a 7.6 yr Orbit around Sgr A*. The Astrophysical Journal **899**(1), 50 (2020) https://doi.org/10.3847/1538-4357/ab9c1c . Publisher: The American Astronomical Society

[59] Peiker, F., Eckart, A., Zajaek, M., Britzen, S.: Observation of S4716a Star with a 4 yr Orbit around Sgr A*. The Astrophysical Journal **933**(1), 49 (2022) https://doi.org/10.3847/1538-4357/ac752f . Publisher: The American Astronomical Society

[60] Abuter, R., Amorim, A., Baubck, M., Berger, J.P., Bonnet, H., Brandner, W., Clnet, Y., Dallilar, Y., Davies, R., Zeeuw, P.T.d., Dexter, J., Drescher, A., Eisenhauer, F., Schreiber, N.M.F., Garcia, P., Gao, F., Gendron, E., Genzel, R., Gillessen, S., Habibi, M., Haubois, X., Heiel, G., Henning, T., Hippler, S., Horrobin, M., Jimnez-Rosales, A., Jochum, L., Jocou, L., Kaufer, A., Kervella, P., Lacour, S., Lapeyrre, V., Bouquin, J.-B.L., Lna, P., Lutz, D., Nowak, M., Ott, T., Paumard, T., Perraut, K., Perrin, G., Pfuhl, O., Rabien, S., Rodrguez-Coira, G., Shangguan, J., Shimizu, T., Scheithauer, S., Stadler, J., Straub, O., Straubmeier, C., Sturm, E., Tacconi, L.J., Vincent, F., Fellenberg, S.v., Waisberg, I., Widmann, F., Wieprecht, E., Wiezorrek, E., Woillez, J., Yazici, S., Zins, G.: Detection of faint stars near Sagittarius A* with GRAVITY. Astronomy & Astrophysics **645**, 127 (2021) https://doi.org/10.1051/0004-6361/202039544 . Publisher: EDP Sciences

[61] Gravity Collaboration, Abd El Dayem, K., Abuter, R., Aimar, N., Amaro Seoane, P., Amorim, A., Beck, J., Berger, J.P., Bonnet, H., Bourdarot, G., Brandner, W., Cardoso, V., Capuzzo Dolcetta, R., Clénet, Y., Davies, R., de Zeeuw, P.T., Drescher, A., Eckart, A., Eisenhauer, F., Feuchtgruber, H., Finger, G., Förster Schreiber, N.M., Foschi, A., Gao, F., Garcia, P., Gendron, E., Genzel, R., Gillessen, S., Hartl, M., Haubois, X., Haussmann, F., Heißel, G., Henning, T., Hippler, S., Horrobin, M., Jochum, L., Jocou, L., Kaufer, A., Kervella, P., Lacour, S., Lapeyrère, V., Le Bouquin, J.-B., Léna, P., Lutz, D., Mang, F., More,

N., Ott, T., Paumard, T., Perraut, K., Perrin, G., Pfuhl, O., Rabien, S., Ribeiro, D.C., Sadun Bordoni, M., Scheithauer, S., Shangguan, J., Shimizu, T., Stadler, J., Straub, O., Straubmeier, C., Sturm, E., Tacconi, L.J., Urso, I., Vincent, F., von Fellenberg, S.D., Widmann, F., Wieprecht, E., Woillez, J., Zhang, F.: Improving constraints on the extended mass distribution in the Galactic center with stellar orbits. A&A **692**, 242 (2024) https://doi.org/10.1051/0004-6361/202452274 arXiv:2409.12261 [astro-ph.GA]

[62] Sadun Bordoni, M., Capuzzo Dolcetta, R., Generozov, A., Bourdarot, G., Drescher, A., Eisenhauer, F., Genzel, R., Gillessen, S., Joharle, S., Mang, F., Ott, T., Ribeiro, D.C., von Fellenberg, S.D.: Impact of a granular mass distribution on the orbit of S2 in the Galactic center. A&A **701**, 89 (2025) https://doi.org/10.1051/0004-6361/202554223 arXiv:2507.01510 [astro-ph.GA]

[63] Heißel, G., Paumard, T., Perrin, G., Vincent, F.: The dark mass signature in the orbit of S2. A&A **660**, 13 (2022) https://doi.org/10.1051/0004-6361/202142114 arXiv:2112.07778 [astro-ph.GA]

[64] Alexander, T.: Stellar Dynamics and Stellar Phenomena Near a Massive Black Hole. ARA&A **55**(1), 17–57 (2017) https://doi.org/10.1146/annurev-astro-091916-055306 arXiv:1701.04762 [astro-ph.GA]

[65] Merritt, D.: Dynamics and Evolution of Galactic Nuclei, (2013)

[66] Vasiliev, E.: A New Fokker-Planck Approach for the Relaxation-driven Evolution of Galactic Nuclei. ApJ **848**(1), 10 (2017) https://doi.org/10.3847/1538-4357/aa8cc8 arXiv:1709.04467 [astro-ph.GA]

[67] Lauer, T.R., Ajhar, E.A., Byun, Y.-I., Dressler, A., Faber, S.M., Grillmair, C., Kormendy, J., Richstone, D., Tremaine, S.: The Centers of Early-Type Galaxies with HST.I.An Observational Survey. AJ **110**, 2622 (1995) https://doi.org/10.1086/117719

[68] Schödel, R., Gallego-Cano, E., Dong, H., Nogueras-Lara, F., Gallego-Calvente, A.T., Amaro-Seoane, P., Baumgardt, H.: The distribution of stars around the Milky Way's central black hole. II. Diffuse light from sub-giants and dwarfs. A&A **609**, 27 (2018) https://doi.org/10.1051/0004-6361/201730452 arXiv:1701.03817 [astro-ph.GA]

[69] Tep, K., Fouvry, J.-B., Pichon, C., Heißel, G., Paumard, T., Perrin, G., Vincent, F.: Mapping the Galactic centre's dark cluster via resonant relaxation. MNRAS **506**(3), 4289–4301 (2021) https://doi.org/10.1093/mnras/stab1945 arXiv:2103.13148 [astro-ph.GA]

[70] Merritt, D., Alexander, T., Mikkola, S., Will, C.M.: Stellar dynamics of extreme-mass-ratio inspirals. Phys. Rev. D **84**(4), 044024 (2011) https://doi.org/10.1103/PhysRevD.84.044024 arXiv:1102.3180 [astro-ph.CO]

[71] Amaro Seoane, P.: Fractional Dynamics in Galactic Nuclei: Non-Local Transport, Transient Phenomena and the Nullification of the Schwarzschild Barrier. arXiv e-prints, 2511–09648 (2025) https://doi.org/10.48550/arXiv.2511.09648 arXiv:2511.09648 [astro-ph.GA]